frontiers in Energy Research

ORIGINAL RESEARCH
published: 20 May 2016
doi: 10.3389/fenrg.2016.00020

Electrochemical Stability of $Li_{6.5}La_3Zr_{1.5}M_{0.5}O_{12}$ (M = Nb or Ta) against Metallic Lithium

*Yunsung Kim[1], Aeri Yoo[2], Robert Schmidt[1], Asma Sharafi[1], Heechul Lee[2], Jeff Wolfenstine[3] and Jeff Sakamoto[1]**

[1] Department of Mechanical Engineering, University of Michigan, Ann Arbor, MI, USA, [2] Department of Advanced Materials Engineering, Korea Polytechnic University, Siheung, South Korea, [3] Army Research Laboratory, RDRL-SED-C, Adelphi, MD, USA

The electrochemical stability of $Li_{6.5}La_3Zr_{1.5}Nb_{0.5}O_{12}$ (LLZNO) and $Li_{6.5}La_3Zr_{1.5}Ta_{0.5}O_{12}$ (LLZTO) against metallic Li was studied using direct current (DC) and electrochemical impedance spectroscopy (EIS). Dense polycrystalline LLZNO (ρ = 97%) and LLZTO (ρ = 92%) were made using sol–gel synthesis and rapid induction hot-pressing at 1100°C and 15.8 MPa. During DC cycling tests at room temperature (± 0.01 mA/cm^2 for 36 cycles), LLZNO exhibited an increase in Li–LLZNO interface resistance and eventually short-circuiting while the LLZTO was stable. After DC cycling, LLZNO appeared severely discolored while the LLZTO did not change in appearance. We believe the increase in Li–LLZNO interfacial resistance and discoloration are due to reduction of Nb^{5+} to Nb^{4+}. The negligible change in interfacial resistance and no color change in LLZTO suggest that Ta^{5+} may be more stable against reduction than Nb^{5+} in cubic garnet versus Li during cycling.

Keywords: garnet stability, LLZO, electrochemical stability, ceramic electrolyte, interfacial resistance

OPEN ACCESS

Edited by:
Xueliang Andy Sun, Western University, Canada

Reviewed by:
Hao Liu, Chinese Academy of Engineering Physics, China
Deyu Qu, Wuhan University of Technology, China

***Correspondence:**
Jeff Sakamoto
jeffsaka@umich.edu

Specialty section:
This article was submitted to Energy Storage, a section of the journal Frontiers in Energy Research

Received: *29 February 2016*
Accepted: *03 May 2016*
Published: *20 May 2016*

Citation:
Kim Y, Yoo A, Schmidt R, Sharafi A, Lee H, Wolfenstine J and Sakamoto J (2016) Electrochemical Stability of $Li_{6.5}La_3Zr_{1.5}M_{0.5}O_{12}$ (M = Nb or Ta) against Metallic Lithium. Front. Energy Res. 4:20. doi: 10.3389/fenrg.2016.00020

INTRODUCTION

Improving the performance and safety of batteries may be achieved through the development and integration of solid-state ceramic electrolytes into solid-state batteries (Salam et al., 1999; Dudney et al., 2015). While numerous solid-electrolytes exhibit high conductivity, few examples of viable bulk-scale solid-state batteries have been reported (Knauth, 2009; Dudney et al., 2015). One of the challenges in developing solid-state batteries stems from the lack of understanding of solid electrode-solid electrolyte interface stability, specifically of the Li metal–solid electrolyte interface. Owing to the electropositive nature of Li, there are few examples of bulk oxide solid-electrolytes that are stable at 0 V versus Li/Li$^+$. The Perovskite-type Li-ion conductor, lithium lanthanum titanate (LLTO), exhibits one of the highest bulk ionic conductivities (~1 mS/cm) at room temperature (RT) (Inaguma et al., 1993). Similarly, Aono et al. (1990) reported NASICON (Na superionic conductor) type $Li_{1.3}M_{0.3}Ti_{1.7}(PO_4)_3$ (M = Al or Sc, LATP) also exhibits high bulk ionic conductivity (0.7 mS/cm) at RT. However, LLTO and LATP contain Ti^{4+}, which spontaneously reduces to Ti^{3+} upon contact with metallic Li. In addition, despite its known stable cycling behavior, Schwöbel et al. (2015) found LIPON decomposed into Li_3PO_4, Li_3P, Li_3N, and Li_2O when paired with a metallic Li anode. Thus, cells using LIPON to enable Li anodes likely form a kinetically limited passivation layer. Recent reports of garnet type electrolyte suggest that the formulation consisting of lithia, lanthania, and

zirconia is stable against metallic Li (Murugan et al., 2007). However, it is known that stoichiometric $Li_7La_3Zr_2O_{12}$ (LLZO) results in the tetragonal polymorph with Li-ion conductivities in the 10^{-5} S/cm range at 25°C (Awaka et al., 2009; Wolfenstine et al., 2012; Thompson et al., 2014). We and others have demonstrated that ~0.4–0.5 mol of Li vacancies are required to stabilize the higher conductivity (~10^{-4} to 10^{-3} S/cm at 25°C) cubic garnet type polymorph (Geiger et al., 2011; Rangasamy et al., 2012; Thompson et al., 2014, 2015). For example, when approximately >0.2 mol of Al^{3+} or Ga^{3+} substitute for Li, >0.4 mol of Li vacancies are created in the LLZO lattice, thus stabilizing the cubic garnet type polymorph (Geiger et al., 2011; Rangasamy et al., 2012). Similarly, when approximately 0.25–0.5 mol of Nb or Ta substitute for Zr, 0.25–0.5 mol of Li vacancies are created, respectively, thus stabilizing the cubic garnet type polymorph (Ohta et al., 2011; Adams and Rao, 2012; Miara et al., 2013). It has been shown that the latter doping scheme (doping on the Zr site) is the approach that results in the highest bulk ionic conductivities approaching 1 mS/cm at 25°C (Ohta et al., 2011; Miara et al., 2013; Thompson et al., 2015). Overall, correlating LLZO formulations with conductivity is reasonably well understood, but understanding the effect of cubic garnet type stabilizing dopants on stability against Li metal is not. Thus, the purpose of this work was to study the electrochemical stability against Li metal for the highest known conductivity garnet type formulations; $Li_{6.5}La_3Zr_{1.5}Nb_{0.5}O_{12}$ (LLZNO) and $Li_{6.5}La_3Zr_{1.5}Ta_{0.5}O_{12}$ (LLZTO).

In this study, cubic garnet type LLZNO and LLZTO powders were synthesized using a sol–gel method taking care to prevent Al contamination. The powders were densified using rapid induction hot-pressing (RIHP) to produce >92% relative density. To achieve high phase purity (e.g., limit the commonly observed pyrochlore $La_2Zr_2O_7$ phase) excess Li_2CO_3 was added after calcination and before hot-pressing. The resulting pellets were characterized in Li–garnet–Li cells for electrochemical stability. Electrochemical impedance spectroscopy (EIS) and direct current (DC) electrochemical techniques were used to characterize interfacial stability. It will be shown that of these two high conductivity garnet type formulations, the Ta dopant is more electrochemically stable against Li metal than Nb.

MATERIALS AND METHODS

Powder Preparation

Cubic Al-free LLZTO and LLZNO with the nominal composition $Li_{6.5}La_3Zr_{1.5}Ta_{0.5}O_{12}$ and $Li_{6.5}La_3Zr_{1.5}Nb_{0.5}O_{12}$ were prepared using a sol–gel synthesis method, respectively (Sakamoto et al., 2013). $LiNO_3{\cdot}x6H_2O$ (x = 0.5, 99.999%, Alfa Aesar), $La(NO_3)_3{\cdot}6H_2O$ (99.9% Sigma Aldrich), $Zr(OH_7C_3)$ (70 wt.% in 1-propanol, Sigma Aldrich), and $Nb(OCH_2CH_3)_5$ (99.95%, Sigma Aldrich) and/or $Ta(CH_3C_2H_2O)_5$ (99.98%, Sigma Aldrich) were used as the sol–gel precursors. 1-propanol (anhydrous 99.7%, Sigma Aldrich) and $CH_3OCH_2CH_2OH$ (2-MOE, anhydrous 99.8%, Sigma Aldrich) were used as a solvent, and acetic acid (AC, 1.0M CH_3COOH, Fluka) was used as a chelating agent. The sol–gel process flow chart is shown in **Figure 1**. The Li and La precursors were dissolved in 1-propanol, and Zr and Nb (or Ta) precursors were dissolved in 2-MOE. After the precursors were dissolved, the solutions were combined and stirred until gelation occurred (approximately 45 min) followed by 12 h of aging to assure the reaction was complete. The gels were dried at room temperature for 9 h followed by drying at 450°C for 4 h under air to eliminate organics. The dried powder was cold-pressed into pellets at 10 MPa in a 2 cm diameter stainless steel die. The cold-pressed pellets were then calcined at 900°C for 4 h in an MgO crucible under air. The heating rate was 5°C/min. After calcination, the pellets were manually crushed with an agate mortar and pestle followed by ball-milling for 15 min at 350 rpm using a planetary mill (PM 100; Retsch, Haan, Germany). 80 mL agate vial and 6 agate balls of 10 mm diameter were used 6 and 11 wt.% excess Li_2CO_3 (99.9% Alfa Aesar) were added to LLZNO and LLZTO, respectively, to compensate for Li loss during calcination and densification.

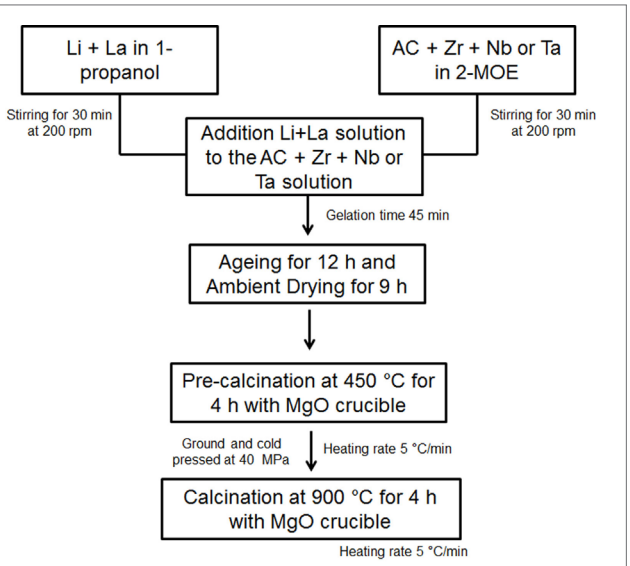

FIGURE 1 | Process flow chart of sol–gel synthesis for $Li_{6.2}La_3Zr_{1.5}Ta_{0.5}O_{12}$ and $Li_{6.2}La_3Zr_{1.5}Nb_{0.5}O_{12}$ powder.

Densification

Al-free LLZNO and LLZTO powders were hot-pressed at 1100°C using a RIHP. A 1.27 cm bore graphite die was used as the susceptor in flowing argon (Rangasamy et al., 2012; David et al., 2015). Since LLZNO and LLZTO powders included excess Li_2CO_3, which melts at ~725°C, a two-step heating profile was used. First, the powder was heated at 1100°C for 15 min without pressure to prevent expulsion of molten Li_2CO_3, followed by the application of 15.8 MPa pressure for 45 min. The cooling rate was 6°C/min. After hot-pressing, each pellet was mounted in Crystalbond® wax and cut into two discs using a diamond saw. To ensure parallel surfaces, the discs were ground with sand paper (400 grit Black ice dry/wet sand paper, Norton Corporation, USA) using a lapping fixture (Model 900; Southbay Technologies, San Clemente, CA, USA) (Kim et al., 2016). The discs were stored in an argon-filled glove box (<1 ppm O_2, <1 ppm H_2O) to minimize surface contamination (Jin and McGinn, 2013; Larraz et al., 2015).

Characterization

The relative densities were defined by dividing the geometric by the theoretical density. The theoretical density was determined by dividing the mass of the atoms in a unit cell by the volume of unit cell determined using X-ray diffraction refinement (XRD, Rigaku Miniflex 600 system, 40 kV and 25 mA).

The phase purity was determined using XRD and Raman spectroscopy (inVia confocal Raman microscope, UK) on of LLZNO and LLZTO before and after cycling test. Raman spectroscopy was performed using a 532 nm green laser and an 1800 line per millimeter holographic grating.

To characterize the stability of the hot-pressed LLZTO and LLZNO samples against Li metal, Li–LLZNO (or LLZTO)–Li symmetric cells were assembled in an argon-filled glove box. To remove the Li_2CO_3 and LiOH surface contamination layers (Jin and McGinn, 2013; Larraz et al., 2015), the hot-pressed LLZNO and LLZTO discs were dry polished with sand paper on a glass plate in the argon-filled glove box. Li foil (Alfa Aesar) was scraped using a spatula to remove the oxide surface layer. A 465 N uniaxial force was applied to the cells and measured using a compression load cell (Omega, LC304-1k, New England, USA).

Direct current cycling was conducted using a potentiostat (VMP300, Bio-Logic, Knoxville) at 23.5 ± 1°C in the argon-filled glove box. Prior to cycling tests, preconditioning cycles were conducted to lower the cell impedance between the LLZNO (or LLZTO) and the Li electrodes. The preconditioning cycles were carried out using ±0.01 mA/cm^2 at 70°C for 10 cycles (each cycle for 2 h). After preconditioning, DC cycling tests were performed at 23.5 ± 1°C for 36 cycles using ±0.01 mA/cm^2. The cell impedance was characterized using EIS between 1 Hz to 7 MHz using the 100 mV perturbation amplitude.

The microstructure of the hot-pressed LLZNO and LLZTO pellets was examined using an optical microscope (Meiji EMZ-13TR, Japan) in the argon-filled glove box.

RESULTS AND DISCUSSION

Materials Characterization

The XRD patterns after hot-pressing for LLZNO and LLZTO with/without 6 and 11 wt.% Li_2CO_3 and the reference pattern for cubic garnet LLZO are shown in **Figure 2**. All the hot-pressed samples consisted of the cubic garnet phase, however some secondary phases were observed in the hot-pressed LLZNO and LLZTO without excess Li_2CO_3. The predominant secondary phase was pyrochlore ($La_2Zr_2O_7$) and was present at ~6.2 and 17.7 wt.% estimated from XRD in LLZNO and LLZTO, respectively. Based on the wt.% fraction of pyrochlore present, the excess Li_2CO_3 required to compensate for Li loss was empirically determined to be 6 and 11 wt.% for LLZNO and LLZTO, respectively. Consequently, the hot-pressed cubic LLZNO and LLZTO with no observable secondary phases were obtained except for a small amount of an unknown phase that was present in the hot-pressed LLZNO with 6 wt.% excess Li_2CO_3 (**Figure 2**). The relative densities of the hot-pressed samples were 97% for LLZNO and 92% for LLZTO.

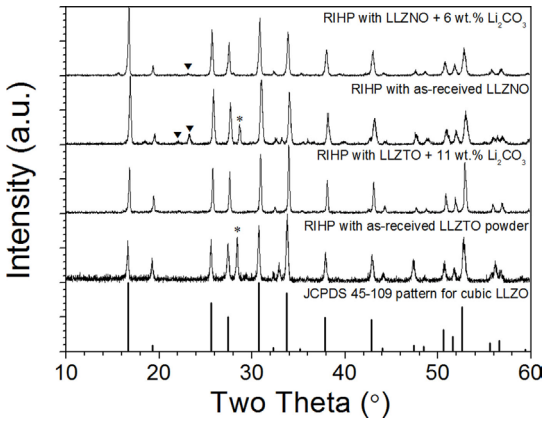

FIGURE 2 | X-ray diffraction patterns of hot-pressed $Li_{6.5}La_3Zr_{1.5}Ta_{0.5}O_{12}$ with 0 and 11 wt.% excess Li_2CO_3, and $Li_{6.5}La_3Zr_{1.5}Nb_{0.5}O_{12}$ with 0 and 6 wt.% excess Li_2CO_3, respectively. *Pyrochlore ($La_2Zr_2O_7$) and ▼ (unknown phase).

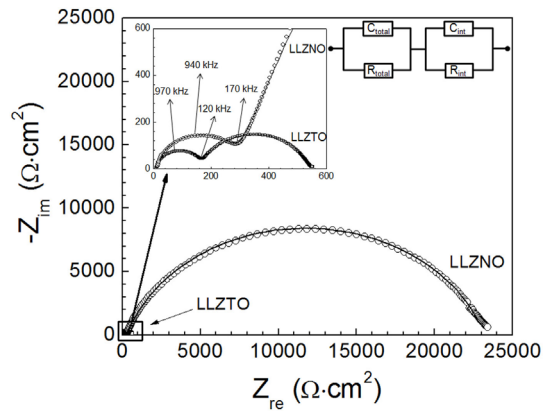

FIGURE 3 | The impedance spectrum with fitted line for as-fabricated Li–LLZNO (or LLZTO)-Li symmetric cells at 23.5 ± 1°C. The solid line corresponds to the fitted the result of the equivalent circuit (○: $Li_{6.5}La_3Zr_{1.5}Nb_{0.5}O_{12}$ and □: $Li_{6.5}La_3Zr_{1.5}Ta_{0.5}O_{12}$).

Initial and after Preconditioning Electrochemical Impedance

Dramatically different cell impedance was observed when comparing LLZNO and LLZTO (**Figure 3**). The impedance spectra are composed of a small semicircle in the high frequency range from 120 kHz to 7 MHz, which is attributed to the total resistance (R_{total}) of the bulk and grain boundaries for the hot-pressed LLZNO (or LLZTO). The relatively large semicircle in the low frequency range between 1 Hz and 120 kHz is attributed to the interfacial resistance (R_{int}) between the hot-pressed LLZNO (or LLZTO) and the Li electrode (**Figure 3**). To determine each impedance and capacitance component, equivalent circuit modeling was conducted. The refined capacitance values for the total resistance of LLZNO (or LLZTO) fall within the range between 10^{-12} and 10^{-8} F/cm^2. In addition, the refined capacitance values

for the interfacial resistance between LLZNO (or LLZTO) and the Li electrodes fall within the range of 10^{-7}–10^{-5} F/cm^2. These values are in agreement with the expected capacitance values of the respective charge transport phenomena (Irvine et al., 1990; Thompson et al., 2014; Sharafi et al., 2016). In addition, the total ionic conductivities were 0.48 and 0.66 mS/cm for the hot-pressed LLZTO and LLZNO calculated from the resistance values ($R_{LLZTO} = 156.1\ \Omega\ cm^2$ and $R_{LLZNO} = 280.9\ \Omega\ cm^2$), respectively. These values are in agreement with the reported values in the literature (Ohta et al., 2011; Liu et al., 2014). From **Figure 3**, it is observed that interfacial resistances ($R_{int,LLZTO} = 373.6\ \Omega\ cm^2$ and $R_{int,LLZNO} = 22{,}924\ \Omega\ cm^2$) are relatively large compared to the total cell resistances. The large difference in Li electrode interfacial resistance between the Li–LLZTO and Li–LLZNO could be affected by the difference in relative density ($\rho_{LLZTO} = 92\%$ and $\rho_{LLZNO} = 97\%$) of the hot-pressed samples, which would enhance wettability and increase surface area. However, it cannot fully explain the ~61 times higher interfacial resistance of Li–LLZNO compared to that of Li–LLZTO. The cause of this difference will be discussed later. It is known that the Li–garnet interfacial resistance can be reduced by simultaneously heating and cycling (Sharafi et al., 2016). It was suggested that the heat and cycling increased wetting and physical contact between LLZTO (or LLZNO) and the Li electrodes. To emulate previous work, preconditioning was performed at low current density (±0.01 mA/cm^2) for 10 cycles at 70°C. The EIS results after preconditioning are shown in **Figures 4A,B**. A comparison of **Figures 3** and **4** reveals that preconditioning reduced the interfacial resistances by ~39% for the hot-pressed LLZTO (**Figure 4A**) and by ~7% for the hot-pressed LLZNO (**Figure 4B**).

Cycling and Electrochemical Impedance

The results of DC cycling and EIS of the LLZNO and LLZTO cells are shown in **Figure 4**. The EIS spectra were measured after preconditioning (0 cycle), 4, 8, 12, 20, 28, and 36 cycles. From **Figure 4A**, it can be observed that the interfacial resistance of the LLZTO cells remained nearly constant during cycling. It can also be observed that the LLZTO sample exhibited stable DC cycling behavior up to 36 cycles (**Figure 4C**). This suggests that LLZTO is stable against Li during cycling. In contrast, the impedance of the LLZNO cell was dramatically reduced, compared to before preconditioning, after four DC cycles (**Figure 4B**). We believe that the decrease in interfacial resistance during the first four

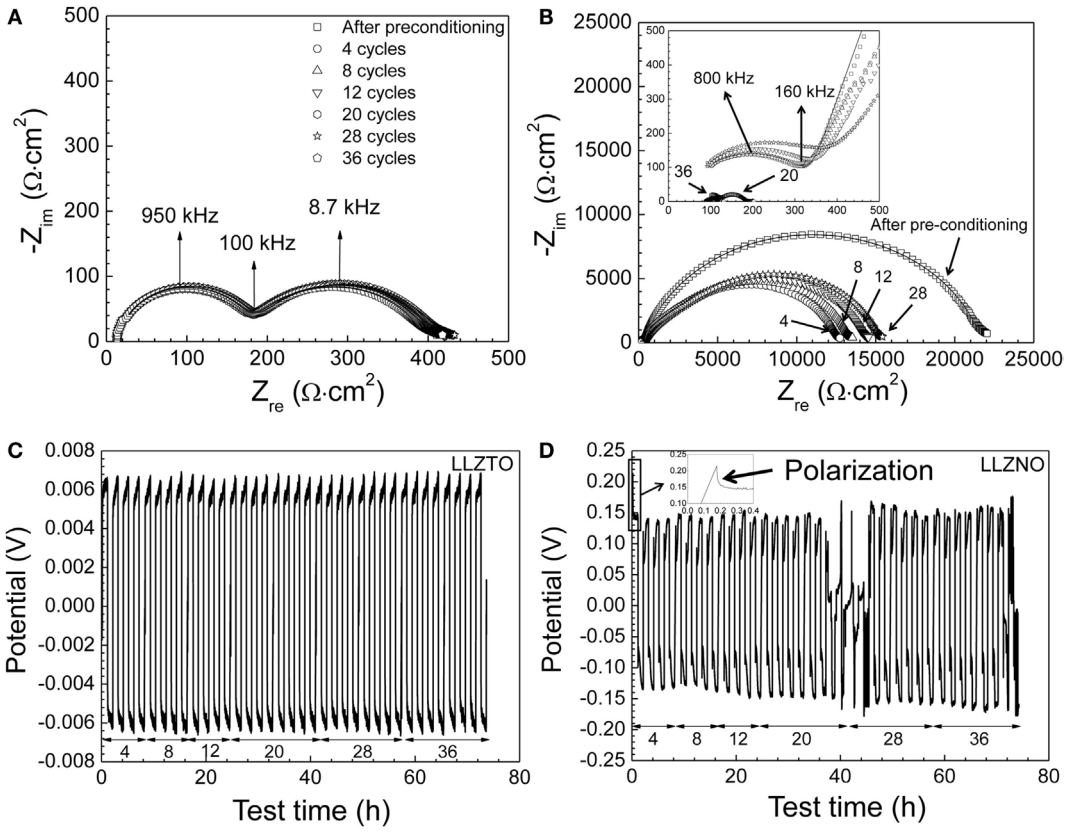

FIGURE 4 | The impedance spectra with fitted line of (A) the Li–$Li_{6.5}La_3Zr_{1.5}Ta_{0.5}O_{12}$–Li cell and (B) the Li–$Li_{6.5}La_3Zr_{1.5}Nb_{0.5}O_{12}$–Li cell as a function of the DC cycling (0, 4, 8, 12, 28, and 36 cycles) at 23.5 ± 1°C, respectively. Since the complexity of the modeling with the $Li_{6.5}La_3Zr_{1.5}Nb_{0.5}O_{12}$ after 4 DC cycles, the modeling with LLZNO was not performed during the cycling tests. The results of the DC cycling for Li–$Li_{6.5}La_3Zr_{1.5}Ta_{0.5}O_{12}$–Li **(C)** and for Li–$Li_{6.5}La_3Zr_{1.5}Nb_{0.5}O_{12}$–Li **(D)** with the 0.01 mA/cm^2 at 23.5 ± 1°C were plotted, respectively. The number of DC cycles was noted below the DC cycling plot.

cycles was due to the plating of Li at the Li–LLZTO interface, which improved contact and reduced interfacial impedance as suggested by Gibson (1976). Gibson (1976) observed a reduction in interfacial impedance after the first few cycles of Na-beta alumina. The increase in impedance with continued cycling suggests that some reaction between LLZNO and Li electrodes had occurred. It is known that Nb^{5+} can be reduced to Nb^{4+} at relatively low potentials (Kodama et al., 2006; Wang et al., 2011). Therefore, the reduction of Nb^{5+} may adversely affect charge transport in LLZNO and/or the formation of a passivating layer. Previous work observed similar behavior in $Li_{6.25}La_3Zr_{1.25}$ $Nb_{0.75}O_{12}$ compared to $Li_{6.25}La_3Zr_{1.25}Ta_{0.75}O_{12}$ (Nemori et al., 2015). Further proof of some interaction between LLZNO and the Li electrodes can observed in **Figure 4D** where short-circuiting of the Li–LLZNO–Li cell occurred during cycling. The potential of the Li–LLZNO–Li cell dramatically decreased after 18 cycles. The occurrence of short-circuiting during DC cycling was in agreement with the EIS measurements (inset in **Figure 4B**) after 20 cycles, where a significant reduction in LLZNO impedance was observed. We believe the short-circuiting was due to the propagation of a Li dendrite through LLZNO (Ishiguro et al., 2013). After 20 cycles, the LLZNO DC cycling behavior was erratic and likely due to Li dendrite forming and breaking-up during continued cycles as observed by Buqa et al. (2005). At cycle 36, a stable Li dendrite likely formed, thus resulting in a short-circuiting.

Characterization after Cycling

The optical images of the hot-pressed LLZTO and LLZNO after 36 cycles of DC cycling are shown in **Figure 5**. Aside from the shiny metallic spots (Li metal) embedded in pores (~8% porosity), there was no evidence of severe discoloration on the surface of the hot-pressed LLZTO before and after DC cycling (**Figure 5A**). Conversely, severe macroscopic discoloration was observed on the surface of the hot-pressed LLZNO (**Figure 5B**). The optical analysis is consistent with the result previously reported by Nemori et al. (2015) and observance of a significant change in the Li–LLZNO impedance spectra (**Figure 4**). The color change in the DC cycled hot-pressed LLZNO confirms that the LLZNO is unstable in contact with Li (**Figure 5B**). Similar discoloration phenomena has been observed in Li_3NbO_4 where darkening, such as the formation of yellow and black regions, resulted from the reduction of Nb^{5+} to Nb^{4+} (Zverev et al., 1972; DeLeo et al., 1988; Nyman et al., 2010). The color change of the hot-pressed LLZNO may be similar to what is observed in the reduction of Nb^{5+} in Li_3NbO_4, which resulted in the loss of Li and/or O. The reduction of Nb^{5+} can affect transport properties (Ishiguro et al., 2013; Nemori et al., 2015), thus a similar phenomenon may occur in the LLZNO causing the interfacial resistance to increase. Conversely, the reduction of Ta^{5+} is less likely compared to Nb^{5+}, which is consistent with the observation that no apparent change in LLZTO was noted in this work (Zverev et al., 1972).

The short-circuiting phenomenon observed during electrochemical characterization (**Figures 4B,D**) also appears to correspond with the optical image of the fracture surface (**Figure 5B**). Macroscopic discoloration was observed on the face and fracture surfaces the hot-pressed LLZNO (**Figure 5B**). Thus, the discoloration through the entire LLZNO pellet could indicate the Li dendrite grew through the hot-pressed LLZNO during cycling test. On the contrary, no color change and/or an evidence of Li dendrite growth were observed on the fracture surface of the hot-pressed LLZTO (**Figure 5A**). These results are in good agreement with the stable DC cycling and EIS behavior up to 36 cycles (**Figures 4A,C**).

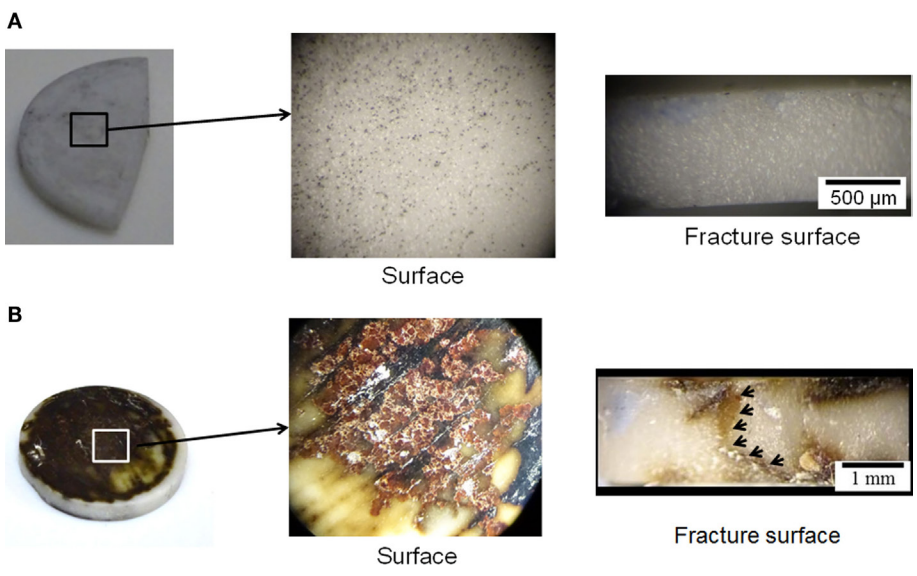

FIGURE 5 | The optical images of the pellet faces and fracture surfaces for the DC cycled hot-pressed (A) $Li_{6.5}La_3Zr_{1.5}Ta_{0.5}O_{12}$ and (B) $Li_{6.5}La_3Zr_{1.5}Nb_{0.5}O_{12}$ after 36 cycles at 23.5 ± 1°C. The arrows indicate the extended dark region across the hot-pressed $Li_{6.5}La_3Zr_{1.5}Nb_{0.5}O_{12}$.

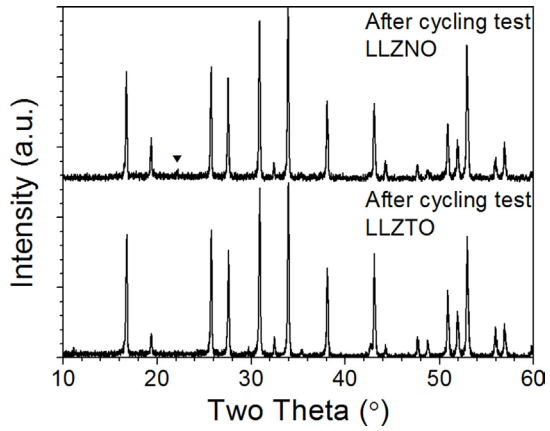

FIGURE 6 | X-ray diffraction patterns of hot-pressed $Li_{6.5}La_3Zr_{1.5}Ta_{0.5}O_{12}$ and $Li_{6.5}La_3Zr_{1.5}Nb_{0.5}O_{12}$ after DC cycling at 23.5 ± 1°C, respectively. ▼ (unknown phase).

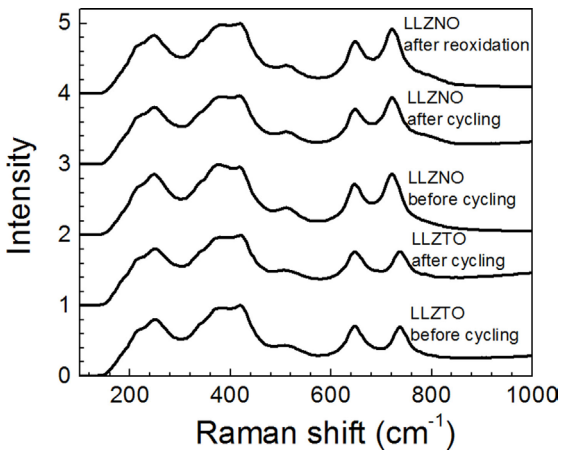

FIGURE 7 | Raman spectra of $Li_{6.5}La_3Zr_{1.5}Ta_{0.5}O_{12}$ and $Li_{6.5}La_3Zr_{1.5}Nb_{0.5}O_{12}$ before and after DC cycling at 23.5 ± 1°C; (top spectrum) LLZNO after DC cycling and after heat treatment at 600°C in air for 2 h.

X-ray diffraction refinement patterns after the 36th cycle for LLZNO and LLZTO are shown in **Figure 6**. No impurity peaks were detected even though the appearance of the hot-pressed LLZNO had undergone significant discoloration after cycling test.

Raman spectroscopy was also conducted to determine if the surface chemistry of LLZNO and LLZTO changed before and after DC cycling (**Figure 7**). The Raman spectra were in good agreement with the results of XRD, which determined that only the cubic garnet phase was present on the surface. In addition, the Raman spectra were consistent with the spectra of cubic LLZTO reported by Thompson et al. (2014). The LLZTO band at ~640 and ~740 cm^{-1} are related with Zr–O bond stretching (Tietz et al., 2013; Larraz et al., 2013) and Ta–O bond stretching (Thompson et al., 2014), respectively. Therefore, the LLZNO band at ~640 and ~720 cm^{-1} of LLZNO can be assigned to the stretching of ZrO_6 and NbO_6 octahedron, respectively. In addition, no peak separation, which could have resulted from the lower symmetry found in the tetragonal phase, was observed in low frequency region (<350 cm^{-1}) after DC cycling. The results of the Raman analysis indicate that the cubic garnet phase was present despite the color change. However, it was possible that the fraction of impurity phases present were too low for detection using conventional benchtop XRD and Raman spectroscopy.

To determine if the LLZNO discoloration after DC cycling was associated with the reduction of Nb^{5+} to Nb^{4+}, the sample was heated in ambient air at 600°C for 2 h. After heating in air, the dark discoloration was converted back to the original white color. In addition, Raman showed no change in the structure after cycling and re-oxidation (**Figure 7**). This suggests that the color change could be associated with a change in valence from Nb^{5+} to Nb^{4+}.

CONCLUSION

The electrochemical stability of the LLZTO and LLZNO against Li was investigated. The LLZTO and LLZNO powders, which were synthesized using sol–gel, were hot-pressed for 1 h at 1100°C, resulting in 92 and 97% relative densities, respectively. The cubic garnet type phase for both LLZTO and LLZNO were obtained by adding excess Li_2CO_3 (6 wt.% for LLZNO and 11 wt.% for LLZTO).

Direct current and EIS were conducted on Li–LLZNO (or LLZTO)–Li cells. Several observations were made from these tests. First, preconditioning at 70°C reduced cell impedance likely due to improved physical contact and wettability between the LLZNO (or LLZTO) and the Li electrode. Second, the resistance of the Li–LLZNO interface significantly decreased after four DC cycles. We believe that electrochemical Li deposition onto the surface resulted in enhanced physical contact between Li and LLZNO compared to the as-assembled cell impedance. Subsequently, the resistance of Li–LLZNO increased with continued DC cycling while that of Li–LLZTO interface remained constant up to 36 DC cycles at 23.5 ± 1°C. Third, LLZNO severely discolored while LLZTO did not change after DC cycling. We believe that the increase in interfacial resistance and discoloration in LLZNO are a result of the reduction of Nb^{5+} to Nb^{4+}. The color change of DC cycled LLZNO from dark to original white after heat treatment at 600°C for 2 h supports the reduction of Nb^{5+} to Nb^{4+} during DC cycling. In contrast, there was no evidence of Ta^{5+} instability in LLZTO after DC cycling. Overall, the results of this study indicate while numerous supervalent dopants can stabilize the high Li-ion conducting garnet phase, not all are stable against reduction in contact with metallic Li.

AUTHOR CONTRIBUTIONS

YK conducted the majority of experiments and wrote the majority of the manuscript. AY synthesized the LLZNO and LLZTO garnet powder by sol–gel. RS performed the part of densification experiments. AS coordinated the electrochemical test conditions

and analysis work. HL designed the sol–gel synthesis process and made intellectual contribution to this work. JW made intellectual contribution and provided background and data analysis of the manuscript. JS designed this work concept and made intellectual contribution and edited the manuscript.

REFERENCES

Adams, S., and Rao, R. P. (2012). Ion transport and phase transition in $Li_{7-x}La_3(Zr_{2-x}M_x)O_{12}$ ($M=Ta^{5+}$, Nb^{5+}, x=0, 0.25). *J. Mater. Chem.* 22, 1426–1434. doi:10.1039/C1JM14588F

Aono, H., Sugimoto, E., Sadaoka, Y., Imanaka, N., and Adachi, G. (1990). Ionic conductivity of solid electrolytes based on lithium titanium phosphate. *J. Electrochem. Soc.* 137, 1023–1027. doi:10.1149/1.2086597

Awaka, J., Kijima, N., Hayakawa, H., and Akimoto, J. (2009). Synthesis and structure analysis of tetragonal $Li_7La_3Zr_2O_{12}$ with the garnet-related type structure. *J. Solid State Chem.* 182, 2046–2052. doi:10.1016/j.jssc.2009.05.020

Buqa, H., Goers, D., Holzapfel, M., Spahr, M. E., and Novak, P. (2005). High rate capability of graphite negative electrodes for lithium-ion batteries. *J. Electrochem. Soc.* 152, A474–A481. doi:10.1149/1.1851055

David, N. I., Thompson, T., Wolfenstine, J., Allen, J. L., and Sakamoto, J. (2015). Microstructure and Li-ion conductivity of hot-pressed cubic $Li_7La_3Zr_2O_{12}$. *J. Am. Ceram. Soc.* 98, 1209–1214. doi:10.1111/jace.13455

DeLeo, G. G., Dobson, J. L., Masters, M. F., and Bonjack, L. H. (1988). Electronic structure of an oxygen vacancy in lithium niobate. *Phys. Rev. B* 37, 8394–8400. doi:10.1103/PhysRevB.37.8394

Dudney, N. J., West, W. C., and Nanda, J. (2015). *Handbook of Solid State Batteries*. Singapore: World Scientific.

Geiger, C. A., Alekseev, E., Lazic, B., Fisch, M., Armbruster, T., Langner, R., et al. (2011). Crystal chemistry and stability of "$Li_7La_3Zr_2O_{12}$" garnet: a fast lithium-ion conductor. *Inorg. Chem.* 50, 1089–1097. doi:10.1021/ic101914e

Gibson A. (1976). "A study of the electrode interface formed between sodium metal and beta alumina solid electrolyte," in *Proc. of the 10th Int. Power Sources Sym*, Brighton, England.

Inaguma, Y., Liquan, C., Itoh, M., Nakamura, T., Uchida, T., Ikuta, H., et al. (1993). High ionic conductivity in lithium lanthanum titanate. *Solid State Ionics.* 86, 689–693. doi:10.1016/0038-1098(93)90841-A

Irvine, J. T. S., Sinclair, D. C., and West, A. R. (1990). Electroceramics: characterization by impedance spectroscopy. *Adv. Mater.* 2, 132–138. doi:10.1002/adma.19900020304

Ishiguro, K., Nakata, Y., Matsui, M., Uehi, I., Takeda, Y., Yamamoto, O., et al. (2013). Stability of Nb-doped cubic $Li_7La_3Zr_2O_{12}$ with lithium metal. *J. Electrochem. Soc.* 160, A1690–A1693. doi:10.1149/2.036310jes

Jin, Y., and McGinn, P. J. (2013). $Li_7La_3Zr_2O_{12}$ electrolyte stability in air and fabrication of a Li/$Li_7La_3Zr_2O_{12}$/Cu0.1V2O5 solid-state battery. *J. Power Sources* 239, 326–331. doi:10.1016/j.jpowsour.2013.03.155

Kim, Y., Jo, H., Allen, J. L., Choe, H., Wolfenstine, J., and Sakamoto, J. (2016). The effect of relative density on the mechanical properties of hot-pressed cubic $Li_7La_3Zr_2O_{12}$. *J. Am. Ceram. Soc.* 99, 1367–1374. doi:10.1111/jace.14084

Knauth, P. (2009). Inorganic solid Li ion conductors: an overview. *Solid State Ionics.* 180, 911–916. doi:10.1016/j.ssi.2009.03.022

Kodama, R., Terada, Y., Nakai, I., Komaba, I., Komaba, S., and Kumagai, N. (2006). Electrochemical and in situ XAFS-XRD investigation of Nb_2O_5 for rechargeable lithium batteries. *J. Electrochem. Soc.* 153, A583–A588. doi:10.1149/1.2163788

Larraz, G., Orera, A., and Sanjuan, M. L. (2013). Cubic phases of garnet-type $Li_7La_3Zr_2O_{12}$: the role of hydration. *J. Mater. Chem.* A1, 11419–11428. doi:10.1039/C3TA11996C

Larraz, G., Orera, A., Sanz, J., Sobrados, I., Diez-Gomez, V., and Sanjuan, M. L. (2015). NMR study of Li distribution in $Li_{7-x}H_xLa_3Zr_2O_{12}$ garnets. *J. Mater. Chem. A* 3, 5683–5691. doi:10.1039/C4TA04570J

Liu, K., Ma, J. T., and Wang, C. A. (2014). Excess lithium salt functions more than compensating for lithium loss when synthesizing $Li_{6.5}La_3Ta_{0.5}Zr_{1.5}O_{12}$ in alumina crucible. *J. Power Sources* 260, 109–114. doi:10.1016/j.jpowsour.2014.02.065

Miara, L. J., Ong, S. P., Mo, Y., Richards, D. R., Park, Y., Lee, J. M., et al. (2013). Effect of Rb and Ta doping on the ionic conductivity and stability of the garnet $Li_{7+2x-y}(La_{3-x}Rb_x)(Zr_{2-y}Ta_y)O_{12}$ ($0\leq x\leq 0.375$, $0\leq y\leq 1$) superionic conductor: a first principles investigation. *Chem. Mater.* 25, 3048–3055. doi:10.1021/cm401232r

Murugan, R., Thangadurai, V., and Weppner, W. (2007). Fast lithium ion conduction in garnet-type $Li_7La_3Zr_2O_{12}$. *Angew. Chem. Int. Ed.* 46, 7778–7781. doi:10.1002/anie.200701144

Nemori, H., Matsuda, Y., Mitsuoka, S., Matsui, M., Yamamoto, O., Takeda, Y., et al. (2015). Stability of garnet-type solid electrolyte $Li_xLa_3A_{2-y}B_yO_{12}$ (A=Nb or Ta, B=Sc or Zr). *Solid State Ionics.* 282, 7–12. doi:10.1016/j.ssi.2015.09.015

Nyman, M., Alam, T. M., McIntyre, S. K., Bleier, G. C., and Ingersoll, D. (2010). Alternative approach to increasing Li mobility in Li-LaNb/Ta garnet electrolytes. *Chem. Mater.* 22, 5401–5410. doi:10.1021/cm101438x

Ohta, S., Kobayashi, T., and Asaoka, T. (2011). High lithium ionic conductivity in the garnet-type oxide $Li_{7-x}La_3(Zr_{2-x}, Nb_x)O_{12}$ (X=0-2). *J. Power Sources* 196, 3342–3345. doi:10.1016/j.jpowsour.2010.11.089

Rangasamy, E., Wolfenstine, J., and Sakamoto, J. (2012). The role of Al and Li concentration on the formation of cubic garnet solid electrolyte of nominal composition $Li_7La_3Zr_2O_{12}$. *Solid State Ionics.* 206, 28–32. doi:10.1016/j.ssi.2011.10.022

Sakamoto, J., Rangasamy, E., Kim, H., Kim, Y., and Wolfenstine, J. (2013). Synthesis of nano-scale fast ion conducting cubic $Li_7La_3Zr_2O_{12}$. *Nanotechnology* 24, 424005. doi:10.1088/0957-4484/24/42/424005

Salam, F., Brike, P., and Weppner, W. (1999). Solid-state CO_2 sensor with Li_2CO_3-MgO electrolyte and $LiMn_2O_4$ as solid reference electrode. *Electrochem. Solid State Lett.* 2, 201–204. doi:10.1149/1.1390783

Schwöbel, A., Hausbrabd, R., and Jaegermann, W. (2015). Interface reaction between LIPON and lithium studied by in-situ X-ray photoemission. *Solid State Ionics.* 273, 51–54. doi:10.1016/j.ssi.2014.10.017

Sharafi, A., Meyer, H. M., Nanda, J., Wolfenstine, J., and Sakamoto, J. (2016). Characterizing the Li-$Li_7La_3Zr_2O_{12}$ interface stability and kinetics as a function of temperature and current density. *J. Power Sources* 302, 135–139. doi:10.1016/j.jpowsour.2015.10.053

Thompson, T., Sharafi, A., Johannes, M. D., Huq, A., Allen, J. L., Wolfenstine, J., et al. (2015). A tale of two sites: on defining the carrier concentration in garnet-based ionic conductors for advanced Li batteries. *Adv. Energy Mater.* 1500096, 1–9. doi:10.1002/aenm.201500096

Thompson, T., Wolfenstine, J., Allen, J. L., Johannes, M., Huq, A., David, I. N., et al. (2014). Tetragonal vs. cubic phase stability in Al-free Ta doped $Li_7La_3Zr_2O_{12}$. *J. Mater. Chem. A* 2, 13431–13436. doi:10.1039/C4TA02099E

Tietz, F., Wegener, T., Gerhards, M. T., Giarola, M., and Mariotto, G. (2013). Synthesis and Raman micro-spectroscopy investigation of $Li_7La_3Zr_2O_{12}$. *Solid State Ionics* 230, 77–82. doi:10.1016/j.ssi.2012.10.021

Wang, X. J., Krumeich, F., Worle, M., Nesper, R., Jantsky, L., and Fiellvag, H. (2011). Niobium(V) oxynitride: synthesis, characterization, and feasibility as anode material for rechargeable lithium-ion batteries. *Chem. Eur. J.* 18, 5970–5978. doi:10.1002/chem.201102653

Wolfenstine, J., Rangasamy, E., Allen, J. L., and Sakamoto, J. (2012). High conductivity of dense tetragonal $Li_7La_3Zr_2O_{12}$. *J. Power Sources* 208, 193–196. doi:10.1016/j.jpowsour.2012.02.031

Zverev, G. M., Levchuk, E. A., Pashkov, V. A., and Poryadin, Y. D. (1972). Laser-radiation-induced damage to the surface of lithium niobate and tantalite single crystals. *Sov. J. Quantum Electron.* 2, 167–169. doi:10.1070/QE1972v002n02ABEH004409

FUNDING

YK, RS, AS, JW, and JS would like to acknowledge support from the Advanced Research Projects Agency-Energy (DE-AR0000399) and from Department of Energy (DE-EE-00006821).

Conflict of Interest Statement: The authors declare that the research was conducted in the absence of any commercial or financial relationships that could be construed as a potential conflict of interest.